J Mater Sci (2011) 46:1161–1166
DOI 10.1007/s10853-010-4886-5

A study on the hardness and elastic modulus of friction stir welded aluminum alloy thick plate joints using micro-indentation

Weifeng Xu · Jinhe Liu · Hongqiang Zhu

Received: 3 July 2010 / Accepted: 28 August 2010 / Published online: 16 September 2010

Abstract Micro-indentation technique was employed to study the hardness and elastic modulus for different positions along the thickness of weld nugget zone (WNZ) in friction stir welded aluminum alloy thick plate joints and base material (BM). Experimental results showed that maximum hardness and elastic modulus 2.11 and 81.6 GPa were obtained in the top of WNZ, minimum values 0.79 and 74.9 GPa present in the BM, respectively. For different positions, both of them were as follows: BM < bottom < middle < top. Meanwhile, the hardness decreased with the increase in grain size or the load. The rod-like shape precipitates presented in the BM and the round particles of top was smaller than that of middle and bottom, and the top of WNZ presents the higher dislocation density.

Introduction

Since the beginning of the last century, indention tests have been widely used to characterize the mechanical properties of material. The development of micro-indentation enables us to investigate the material properties at the micro scales [1]. Compared with the conventional Vickers micro-hardness testing, Uzun et al. [2] mentioned that the depth-sensing micro-indentation method offers great advantages in two aspects. First, apart from micro-hardness, the method can also provide well-defined mechanical parameters such as elastic modulus of the interfacial zone. Secondly, as load and depth of an indentation are continuously monitored, optical observation and measurement of diagonal length of the indent or impression are no longer required because they can be difficult and subjected to inaccuracy.

Hardness behavior of material is normally related to its resistance to plastic deformation usually by indentation. Moreover, hardness is a mechanical parameter, which is strongly related to the structure and composition of solids. Hence, hardness is not only a mechanical characteristic routinely measured, but also it has been developed as an investigation method for structural parameters in recent years [3]. The material properties such as the elastic modulus (which is the characterization of materials on the elastic deformation of the resistance) change with large plastic deformation and precise measurement for the material properties is strongly required by Yang et al. [4].

2××× series aluminum alloys were commonly used in the aerospace industry due to its light weight, specific strength, and stiffness, but the strength of joints using the conventional fusion welding only reaches 50–70% of the parent metal and readily form flaws (such as voids and hot cracks, etc.). Friction stir welding (FSW) is a new process, having been invented in 1991 [5], and unlike conventional fusion welding, it is a solid-state process. The FSW process offers several advantages and significantly improves weld properties and has been extensively applied in joining light metals. However, due to the basic principle of FSW and the characteristic frictional heat and stir of welding tool, a large temperature gradient and different amounts of stir along the thickness of plate present when welding thick plate. This inherent asymmetry of the FSW process can produce differences in the microstructure and properties along the thickness of plate [6, 7]. Venkateswaran et al. [8] evaluated the mechanical properties of FSW joints at the interface between heat-treated Al–Mg–Si and strain-hardened Mg–Al–Zn alloy sheets, including the fracture

W. Xu (✉) · J. Liu · H. Zhu
School of Materials and Engineering, Northwestern Polytechnical University, Xi'an 710072, People's Republic of China
e-mail: xwf1982@mail.nwpu.edu.cn

toughness. The fracture toughness (KIC) calculation by both the micro and nano-indentation methods showed very low values, which is the primary reason for the brittle failure of the dissimilar weld joints and concomitant low tensile strengths. Ball indentation technique (BIT) is employed to study the effect of post-weld heat treatment on the mechanical properties of a high strength low alloy [9]. Few studies, however, have focused on the mechanical properties at the micro-scales of materials in different positions along the thickness of weld nugget zone (WNZ).

In this study, the mechanical properties (hardness and elastic modulus) at the micro-scales for the different positions (top, middle, and bottom) along the thickness of WNZ in friction stir welded 2219-O aluminum alloy thick plate and base material (BM) using the micro-indentation have been investigated. Meanwhile, the effect of different grain size and second phase particle distribution on the mechanical properties at the micro-scales was also studied.

Theoretical background

Two mechanical properties of micro-area for the specimen, namely, hardness H and elastic modulus E can be obtained with the load and penetration depth data. It is now generally realized that a crucial step in analyzing the load–penetration curve of micro-indentation is to determine the true contact area. For an ideal sharp Berkovich indenter, the contact area A_c is given by [10]:

$$A_c = 24.56h_c^2 \tag{1}$$

The hardness H usually defined as the ratio of the peak indentation load P_{max} to the project area of hardness impression A_c according to the Oliver–Pharr method [11].

$$H = \frac{P_{max}}{A_c} = \frac{P_{max}}{24.56h_c^2} \tag{2}$$

The procedure of Oliver–Pharr method analysis begins by fitting the unloading curve to an empirical power–law relation [10, 12].

$$P = B(h - h_f)^m \tag{3}$$

where P is the indention load, h the indenter depth, h_f the final depth of contact impression after unloading, B and m are empirically determined fitting parameters. Once the parameters B and m are obtained by curve fitting, the contact stiffness S can be established by Eq. 4.

$$S = \frac{dP}{dh} = mB(h - h_f)^{m-1} \tag{4}$$

The reduced modulus E_r accounts for the effect of a non-rigid indenter on the load–displacement behavior and is computed as

$$E_r = \frac{\sqrt{\pi}}{2} S \frac{1}{\sqrt{A_c}} \tag{5}$$

$$\frac{1}{E_r} = \frac{1 - v^2}{E} + \frac{1 - v_0^2}{E_0} \tag{6}$$

where the E and υ are the Young's modulus and Possion's ratio for the specimen ($E = 73.8$ GPa, $\upsilon = 0.33$), and E_0 and υ_0 are the same parameters for the indenter. For a Berkovich diamond indenter used in this study, $E_0 = 1141$ GPa, $\upsilon_0 = 0.07$.

Materials and experiments

The BMs used in this study are 14-mm-thick aluminum alloy 2219-O rolled plates with the normal composition (in wt%) of Cu—6.48, Mn—0.32, Fe—0.23, Ti—0.06, V—0.08, Zn—0.04, Si—0.49, Zr—0.2, rest—Al. The welding samples, 240 mm × 150 mm, were longitudinally butt welded using the FSW machine. A welding tool with a shoulder of 28 mm and a coniform threaded pin of 12 mm (root) and 7.6 mm (head) in the diameter and 13.6 mm in the length was used. The rotary speed and traverse speed were 400 rpm and 60 mm/min, respectively. The direction of welding was perpendicular to the rolling direction. The WNZ was sliced three zones (top, middle, and bottom) along the thickness plate using the electrospark wire-electrode cutting, which were polished with a diamond paste and etched with Keller's reagent.

The micro-indentation experiments were performed at the Micro Scratch Tester, using Berkovich indenter tip. The indentation procedure used as following: loading to the maximum load at constant loading rate 9.6841 mN/s, holding for the maximum 5 s, and then unloading in approximately the same rate. Micro-indentations are sufficiently spaced so that the indentation behavior is not affected by the presence of adjacent indentations. The measurements were repeated thrice for each condition, an average value was determined on the basis of the three measured data.

Specimens from the WNZ were prepared for transmission electron microscopy (TEM) examination in a JEM-3010 by electropolishing in a 30% nitric acid + 70% methanol solution at 12 V and −30 °C.

Results and discussion

Typical load–displacement curves obtained for the different positions along the thickness of WNZ and BM at a constant maximum loads 50 mN are shown in Fig. 1. The corresponding experimental data are shown in Table 1.

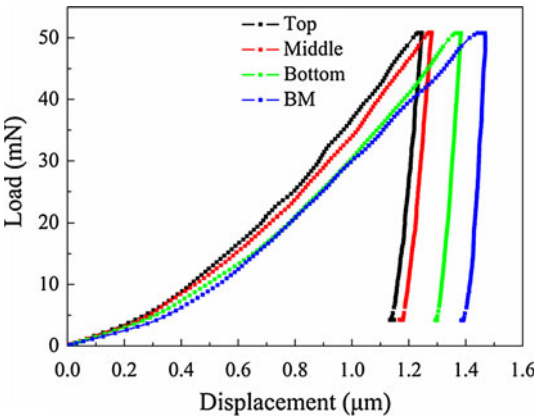

Fig. 1 Load–displacement curves obtained at the same load 50 mN on the different positions along the thickness of WNZ and BM

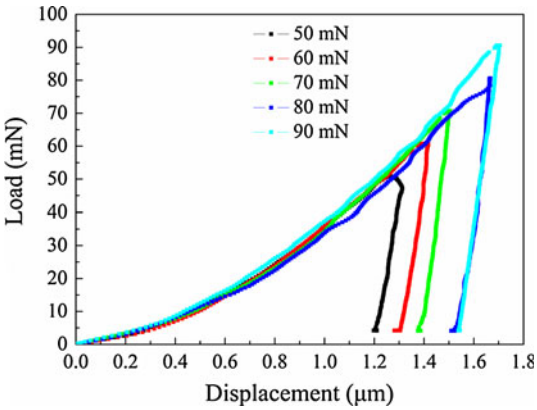

Fig. 2 Load–displacement curves obtained at different maximum loads on the same grain for the top of WNZ

Table 1 The average hardness H and elastic modulus E at a constant load of 50 mN derived from Oliver and Pharr's power law fitting method for different position of samples

	Top	Middle	Bottom	BM
Hardness (GPa)	2.11	1.9	1.6	0.79
Elastic modulus (GPa)	81.6	79.9	75.5	74.9

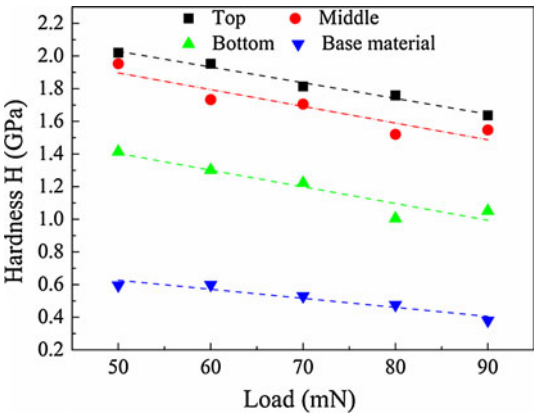

Fig. 3 Plots of hardness versus load of BM and different positions of the WNZ at the different maximum loads

It can be seen that the maximum indentation depth is located in the BM and the depth decreases from bottom to top. Figure 2 shows a typical experimental load–displacement curves obtained at different maximum loads on the same grain. The indentation depth increases with the increase in test force from 50 to 90 mN. From Figs. 1 and 2, it can be found that the pop-in events had not occurred due to the smooth curves during the loading stages. The unloading deformation shows good linear characteristics from the starting points even down to nearly 10% of the peak loading points. The good linearity demonstrated by the unload curves enabled us to use Oliver and Pharr method to calculate the elastic modulus.

Figure 3 shows the hardness of BM and different positions along the thickness of the WNZ determined from Eqs. 1 and 2. Compared with the average hardness of BM (0.52 GPa), the average hardness of WNZ presents significance increase, the average hardness of top (1.84 GPa) is higher than that of middle (1.69 GPa) or bottom (1.2 GPa). The average hardness is as follows: BM < bottom < middle < top. The difference hardness is significant, which shows that the anisotropy is strong in the BM and different positions along the thickness of WNZ. It needs to emphasize that the different positions along the thickness of WNZ present different hardness, which means the heterogeneous microstructure caused by the asymmetrical stirring and the weld thermal cycle along the thickness of plate. Meanwhile, the whole hardness presents a downtrend with the increase in load from 50 to 90 mN.

Table 1 shows the hardness H and elastic modulus E at constant load 50 mN derived from Oliver and Pharr's power law fitting method. It can be found that the average hardness is 2.11, 1.9, 1.6, and 0.79 GPa in the top, middle, bottom of WNZ, and BM, respectively. All of the average hardness values are slightly bigger than that of the results obtained at different maximum loads. It can be found from Fig. 3 and Table 1 that the hardness decreases with the increase in indentation depth or load. At the micro-scales the hardness depends on the indentation depth or load, exhibiting the well-known indentation size effect (ISE). This phenomenon has been presented in numerous micro-indentation tests on various materials such as metals, polymers, ceramics, etc. [1]. Nix and Gao [13] have developed a mechanism-based strain gradient model to rationalize the ISEs (i.e., the load) and obtain the following characteristic expression $H = H_0\sqrt{1 + h^*/h}$ for the depth dependence of hardness. Where H is the hardness for a given indent depth h, H_0 the size independent hardness, and

h^* is characteristic length parameter that characterizes the depth dependence of the hardness. This model predicts that the square of the hardness should be linearly related to the reciprocal of the indentation depth, i.e., the linear relationships are obtained between H^2 and $1/h$. In this study, the linear relationship is in great agreement with the plots of data obtained from experimental results.

The values of E in different positions were obtained according to Eq. 6, which was also shown in Table 1. It can be seen that the value of E is 74.9 GPa in the BM, the corresponding value is 81.6, 79.9, and 75.5 GPa in the top, middle, and bottom, respectively. The E of the material depends on itself crystal characteristics, which reflects the crystal atomic binding forces. The size of the diameter and volume of atomic directly reflect the density of atomic arrangement. Compared to the BM, the WNZ experienced larger plastic deformation during the FSW process, which results in increasing the density of atomic arrangement, and then the atomic binding force enhances, i.e., the increase in elastic modulus. In terms of the solid solution alloys, it has been known that elastic modulus increases with the increase in the valence or when the solute atomic radius is smaller than that of solvent. The radius of Cu and Al is 0.1278 and 0.2860 nm, their valence is +2 and +3 for using Al–Cu series aluminum alloys in this experiment, respectively. The solid solubility of Cu atomic has been improved in the Al matrix after experiencing that the FSW process results in the enhancement of elastic modulus. Meanwhile, the solid solubility of Cu atomic is higher in the top than that in the middle and bottom because of experiencing the higher thermal cycle and the larger plastic deformation.

Figure 4 shows a typical experimental constant loading rate and maximum loads' (50 mN) load–displacement curves obtained at different grain sizes for the top of sample. With the increase in grain size, both the indentation depth and the residual impressions size (10.17 μm → 10.36 μm → 11.12 μm → 12.66 μm) increase. The hardness calculated using the Oliver–Pharr method is 2.16, 2.13, 2.11, and 2.05 GPa for the different grain sizes, respectively. It can be found that the hardness also presents the same trend with the change of grain size, resulting from the increasing hardness toward smaller grain sizes is attributed to dislocation pile-ups at the grain boundaries and improves the deforming resistance, i.e., the plastic deformation is difficult to carry out and the effect of grain-boundary strengthening enhances. Which is in agreement with the smaller grain size and the higher hardness according to Hall–Petch relationship ($H = H_0 - k_H d^{-1/2}$, where H is the hardness, d grain size, and both H_0 and k_H are constant value.), this is in good agreement with [14]. (The hardness was found to be essentially related to grain size through the Hall–Petch relationship in the stir zone.)

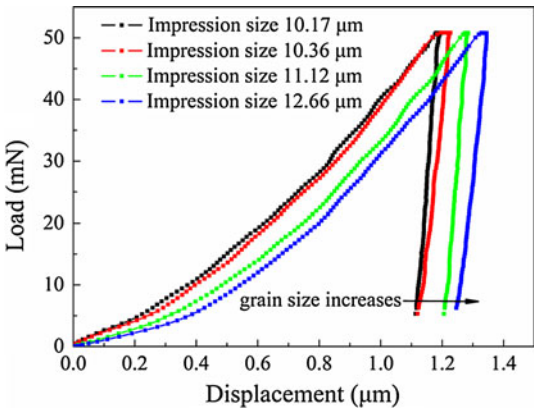

Fig. 4 Load–displacement curves at constant loading rate and maximum loads (50 mN) obtained at different grain size in the top of sample

Figure 5 illustrates the precipitates morphology and distribution in the different regions. TEM bright field images in Fig. 5a show that the rod-shaped precipitates cover the grain matrix. For the WNZ, the precipitates morphology and distribution are strongly dependent on the local thermo-mechanical cycle experienced during FSW. Precipitates in the WNZ appear to have gone into solution and re-precipitated during the weld thermal cycle, the precipitates' redistribution is strongly dependent on the dislocation density [15, 16]. So, the precipitation features in the WNZ present similar morphology, most of them are round particles (small dark dots). Compared to the middle, bottom of WNZ, and BM, the top experiences the greatest degree of mechanical stir and highest temperature generated by the process [6]. Therefore, the top of WNZ contains a larger number of dislocations (black line segments, see Figs. 5 and 6) than that of middle, bottom, and BM, the size of precipitation in the top is smaller and more diffuse distribution. The results further indicate that the hardness is in the following sequence: BM < bottom < middle < top.

Conclusion

In summary, the following conclusions are reached:

1. Compared to the average hardness of BM (0.52 GPa), the top is 1.84 GPa and is higher than that of middle of 1.69 GPa or bottom of 1.2 GPa at different loads. The hardness is 2.11, 1.9, 1.6, and 0.79 GPa in the top, middle, bottom of WNZ, and BM at a constant load of 50 mN, respectively. The hardness decreases with the increase in load, which exhibits the well-known ISE. The corresponding elastic modulus is 81.6, 79.9, 75.5, and 74.9 GPa in the top, middle, bottom, and BM, respectively. Both of the average hardness and elastic modulus are as follows: BM < bottom < middle < top.

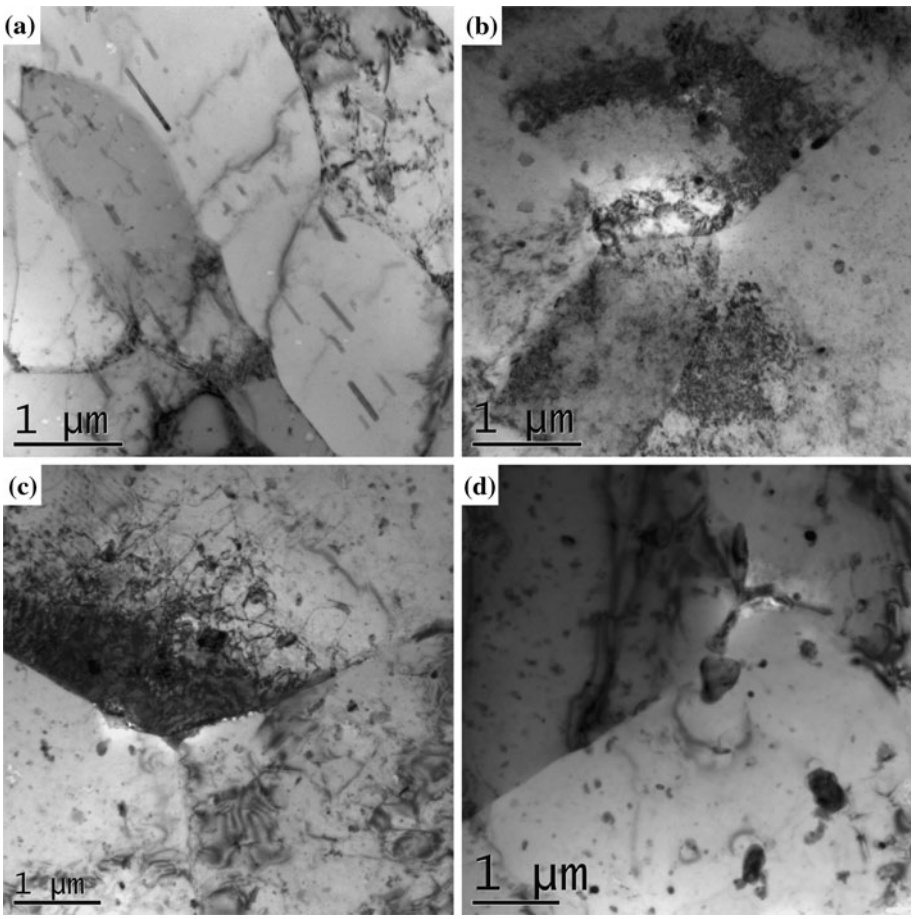

Fig. 5 TEM micrographs of precipitates in BM (**a**) and the different position of the WNZ: **b** top, **c** middle, and **d** bottom

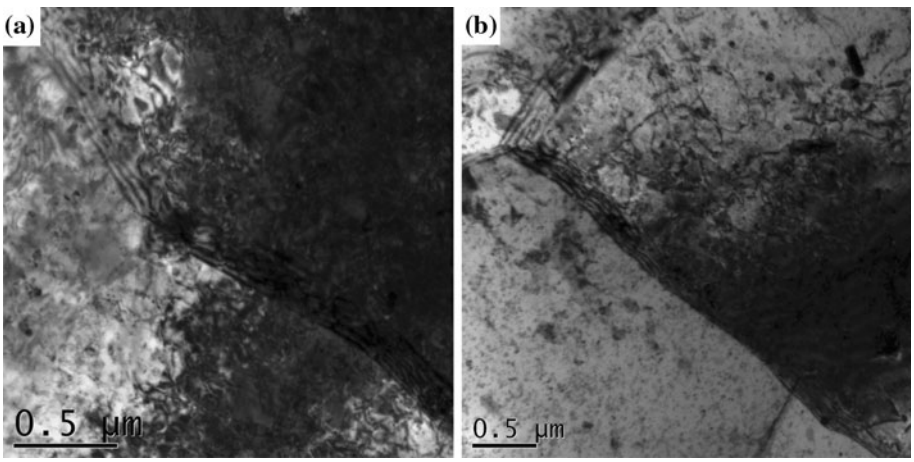

Fig. 6 TEM micrographs of dislocation in the different positions of the WNZ: **a** top and **b** bottom

2. With the increase in grain size, both the indentation depth and the residual impressions size increase and the hardness is 2.16, 2.13, 2.11, and 2.05 GPa, respectively. The trend is in good agreement with the Hall–Petch relationship.
3. The rod-like shape precipitates present in the BM and the different positions along the thickness of WNZ present similar morphology, most of them are small round particles. The top is smaller and more diffuse distribution than that of the middle and bottom. Meanwhile, the top of WNZ presents the higher dislocation density.

References

1. Zhang TY, Xu WH, Zhao MH (2004) Acta Mater 52:57
2. Uzun O, Kolemen U, Celebi S, Guclu N (2005) J Eur Ceram Soc 25:969

3. Culha O, Toparlia M, Sahinb S, Aksoy T (2008) J Mater Process Technol 206:231
4. Yang M, Akiyama Y, Sasaki T (2004) J Mater Process Technol 151:232
5. Thomas WM, Nicholas ED, Needham JC, Murch MG, Temple-Smith P, Dawes CJ (1995) International Patent No. PCT/GB92/02203; GB Patent No. 9,125,978.8, 1991; US Patent No. 5,460,317, 1995
6. Xu WF, Liu JH, Luan GH, Dong CL (2009) Mater Design 30:1886
7. Zhang Z (2008) J Mater Sci 43:5867. doi:10.1007/s10853-008-2865-x
8. Venkateswaran P, Xu ZH, Li XD, Reynolds AP (2009) J Mater Sci 44:4140. doi:10.1007/s10853-009-3607-4
9. Ghosh S, Pal TK, Mukherjee S, Das G, Ghosh S (2008) J Mater Sci 43:5474. doi:10.1007/s10853-008-2840-6
10. Dwyer-Joyce RS, Ushijima Y, Murakami Y, Shibuta R (1998) Tribol Int 31:525
11. Oliver WC, Pharr GM (1992) J Mater Res 7:1564
12. Zeng K, Chiu CH (2001) Acta Mater 49:3539
13. Nix WD, Gao H (1998) J Mech Phys Solids 46:411
14. Xu WF, Liu JH, Luan GH, Dong CL (2008) Acta Metall Sin 44:1404
15. Su JQ, Nelson TW, Mishra R, Mahoney M (2003) Acta Mater 51:713
16. Safarkhanian MA, Goodarzi M, Boutorabi SMA (2009) J Mater Sci 44:5452. doi:10.1007/s10853-009-3735-x